Determining the criticality assessment of defects on wind turbine components detected by UAV sensors*

Serhii Svystun[1,†], Oleksandr Melnychenko[1,†], Pavlo Radiuk[1,*,†], Andrii Lysyi[1,†] and Anatoliy Sachenko[2,3,†]

[1] *Khmelnytskyi National University, 11, Institutes str., Khmelnytskyi, 29016, Ukraine*
[2] *Casimir Pulaski Radom University, 29, Malczewskiego str., Radom, 26-600, Poland*
[3] *West Ukrainian National University, 11, Lvivska str., Ternopil, 46009, Ukraine*

Abstract

Wind turbines often operate in remote and harsh environments, making it difficult to detect, analyze, and manage defects such as cracks, corrosion, and overheating. This study addresses that challenge by proposing a novel approach that combines multi-sensor unmanned aerial vehicle (UAV) inspections with deep learning–based defect recognition and a fuzzy logic approach to assess criticality. The main problem lies in translating raw UAV-collected data into reliable and quantifiable metrics for defect severity, a gap that has inhibited timely interventions and thorough maintenance strategies. This study aims to improve the speed and accuracy of detecting and ranking anomalies in wind turbine blades, towers, and motor assemblies. Experiments show that our proposed multisensor pipeline, which merges thermal and visual data via an ensemble of convolutional neural networks (CNNs), raises detection accuracy by up to 13.5% compared to single-sensor or single-model approaches. Furthermore, the resulting fuzzy-based numerical scores align closely, within 0.15 deviation, with expert judgments of defect urgency. Our conclusions highlight the value of cross-channel data fusion and robust logic-driven rankings for wind energy applications. This approach contributes to reduced operational downtime, improved turbine longevity, and enhanced safety by minimizing overlooked damage and emphasizing prompt and effective maintenance. In summary, the study illustrates how automated UAV data acquisition, ensemble CNN detection, and a systematic fuzzy logic scoring mechanism can work to fill the existing gap in defect criticality assessment on wind power plants.

Keywords

Wind power plants, UAV sensors, defect detection, criticality assessment, fuzzy logic, multispectral fusion, ensemble CNN

1. Introduction

Wind power plants form a key segment of modern renewable energy. Their efficiency and reliability, however, directly depend on the structural integrity of components such as blades, towers, and motor assemblies. These parts endure continuous mechanical loads, varying weather conditions, and corrosion-inducing environments [1]. Minor cracks, localized corrosion, or small overheating events can quickly escalate into critical threats if not identified and resolved early [2]. Although rapid progress has been made in unmanned aerial vehicle (UAV) technology for inspection [3], many existing techniques focus purely on detection without providing a systemic approach to assessing how critical each identified defect is [4].

Assessing defect criticality via UAVs is essential because the ability to classify defects according to their severity enables targeted maintenance, preempting costly breakdowns. Traditional manual

Intelitsis'25: The 6th International Workshop on Intelligent Information Technologies & Systems of Information Security, April 04, 2025, Khmelnytskyi, Ukraine
* Corresponding author.
† These authors contributed equally.
svystuns@khmnu.edu.ua (S. Svystun); melnychenko@khmnu.edu.ua (O. Melnychenko); radiukp@khmnu.edu.ua (P. Radiuk); andriilysyi@khmnu.edu.ua (A. Lysyi); as@wunu.edu.ua (A. Sachenko)
0009-0009-8210-6450 (S. Svystun); 0000-0001-8565-7092 (O. Melnychenko); 0000-0003-3609-112X (P. Radiuk); 0009-0001-0065-9740 (A. Lysyi); 0000-0002-0907-3682 (A. Sachenko)

inspections can be slow and prone to oversight [5], while single-sensor UAV solutions often fail to detect hidden or subtle issues [6]. Incorporating thermal or multispectral data provides further detail [7], but integrating such diverse channels alongside robust deep learning techniques remains challenging [8]. Given the growing scale of wind energy deployment, there is a pressing need for an automated, integrated pipeline that combines precise detection with reliable evaluation of defect criticality.

The goal of this study is to enhance UAV-based inspections by proposing a comprehensive approach to determining the criticality assessment of defects on components of wind power plants detected by UAV sensors. The objective includes developing and validating an approach that fuses sensor data, ensemble deep learning, and fuzzy logic to produce interpretable severity scores for each defect. To this end, we identify three major contributions:

- An end-to-end approach that processes multispectral UAV data and detects multiple defect types via an ensemble of CNN architectures.
- A structured fuzzy logic subsystem that computes a final numeric criticality score (C_{final}) using both physical and thermal parameters, plus expert weighting.
- A validated demonstration of the approach's effectiveness through experiments comparing standard vs. composited data, and single-model vs. ensemble learning, yielding numerical insights into accuracy gains and improved recall rates.

The remainder of this manuscript is organized as follows. Section 2 surveys related works focusing on deep learning–based wind turbine inspections and fuzzy-logic criticality evaluations. Section 3 details the proposed approach to determining the criticality assessment of defects on components of wind power plants detected by UAV sensors. Section 4 provides a rich overview of experiments, including quantitative comparisons, tables, and figures showcasing how multispectral composition boosts detection metrics. Section 5 outlines advantages, disadvantages, and future research questions related to sensor calibration and real-time implementation. Finally, Section 6 concludes with a forward-looking summary of the major findings, numerical improvements, and pathways for extending this work.

2. Related works

Growing interest in UAV-based defect detection for wind power plants has led to numerous research contributions. Traditional methods employed single-sensor red, green, and blue (RGB) data combined with classic machine learning classifiers [9], including random forest or SVM, to detect anomalies such as cracks or corrosion in blade images [10]. However, studies indicate these approaches fail to accommodate complex scenarios involving varied lighting, shape, and surface conditions [11, 12]. Moreover, handcrafted descriptors often lack robustness when confronted with the heterogeneous characteristics of wind turbine components (WTCs) [13].

With the advent of deep learning, convolutional neural networks (CNNs) proved more effective in capturing intricate, data-driven features from imagery. According to [12], YOLOv8 (You Only Look Once) [14, 15] excels in real-time detection, mapping bounding boxes and classes simultaneously. Other two-stage detectors, notably Faster R-CNN [16] and Cascade R-CNN [17], refine localization accuracy at a cost in speed. Recent CNN variants add segmentation masks that can be critical for measuring defect dimensions [7].

To further boost detection precision, ensemble methods combine multiple CNNs specialized in different defect dimensions or spectral data [8]. For instance, YOLO may capture significant defects quickly, while Cascade R-CNN refines bounding boxes of more minor cracks or corrosion [18, 19]. Voting or weighted non-maximal suppression aggregates these bounding boxes, boosting recall in complex images with glare, shadows, and partial occlusions.

Beyond finding defects, attention has shifted to evaluating criticality. Early threshold-based methods, e.g., labeling cracks above 1 cm as "dangerous," proved oversimplified [20]. Fuzzy logic

might be a solution for bridging numerical data (e.g., defect size, thermal anomalies) with domain knowledge [21]. For instance, in [22], fuzzy membership functions quantify geometry, temperature, or curvature parameters, enabling nuanced severity rankings. While fuzziness better mirrors real-world uncertainty, few fully integrated UAV pipelines incorporate a fuzzy approach to ranking detected defects [23]. This gap underscores the relevance of the proposed approach to determining the criticality assessment of defects on components of wind power plants detected by UAV sensors," as it merges ensemble CNN detection with a fuzzy criticality subsystem.

Based on the survey, this study addresses the overarching issue of translating multi-sensor UAV detection outputs into a structured criticality assessment for each identified defect. To achieve this, several tasks must be completed:

- *Task 1:* Acquire and preprocess UAV data from multiple spectral channels, ensuring alignment between RGB and thermal images.
- *Task 2:* Implement robust ensemble CNNs to detect diverse defect types under real-world conditions.
- *Task 3:* Extract physical metrics (length, area) and thermal indicators (min/max/avg temperature) to characterize each defect.
- *Task 4:* Incorporate fuzzy logic or a similar interpretive mechanism to generate numeric criticality scores reflecting domain expert knowledge.

These tasks guide the development of the introduced approach, described in detail below.

3. Methods and materials

In this section, we detail the proposed approach to determining the criticality assessment of defects on components of wind power plants detected by UAV sensors. The approach integrates three primary stages: (i) data collection and composition from multiple UAV sensors, (ii) ensemble CNN-based defect detection, and (iii) fuzzy logic–driven criticality assessment.

3.1. Block structure and workflow

Figure 1 shows an overview of the proposed multi-block system:

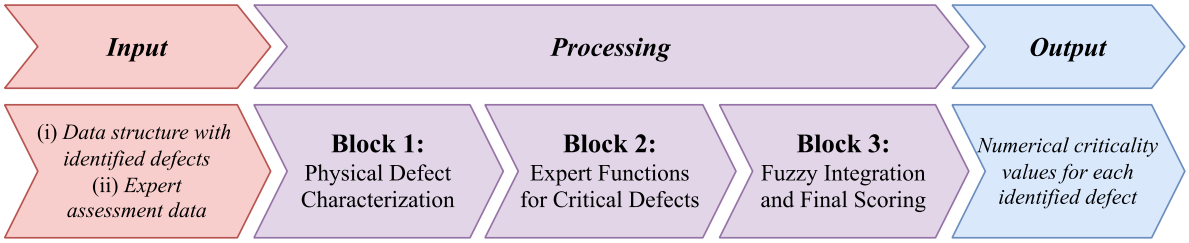

Figure 1: Overall block structure for the proposed approach, combining ensemble CNN detection (not shown here in detail), physical parameter extraction (Block 1), expert severity models (Block 2), and fuzzy logic integration (Block 3).

- *Block 1:* Physical Defect Characterization—Captures raw bounding boxes from the ensemble output, corrects distortions, and computes physical dimensions plus temperature metrics.
- *Block 2:* Expert Functions for Critical Defects—Formalizes cracks, corrosion, and overheating severity via specialized formulas, referencing the tables that assign weighting coefficients (β, γ, η) for each WTC.
- *Block 3:* Fuzzy Integration and Final Scoring—Transforms each detected defect's parameters into fuzzy sets, merges them with expert severity functions, and applies defuzzification to obtain $C_{\text{final}}(D_i)$.

3.2. Block 1: Physical dimensions and thermal analysis

Block 1 implements an iterative process to transform detected bounding boxes into real-world dimensions and temperature profiles.

Step 1.1: Region of Interest (ROI) Extraction. For each detected defect, we crop its region from the undistorted image as follows:

$$I_{\text{ROI}}^{i} = f_{\text{crop}}\left(I_{\text{undistorted}}, x_{\text{ensemble}}^{i}, y_{\text{ensemble}}^{i} + W_{\text{ensemble}}^{i}, y_{\text{ensemble}}^{i} + H_{\text{ensemble}}^{i}\right), \quad (1)$$

where $\left(x_{\text{ensemple}}^{i}, y_{\text{ensemple}}^{i}\right)$ is the bounding box's top-left corner, and $\left(W_{\text{ensemple}}^{i}, H_{\text{ensemple}}^{i}\right)$ are its width and height.

Step 1.2: Image Enhancement (Bilateral Filtering, CLAHE). Noise reduction and local contrast enhancement follow [24], preserving edges while boosting defect visibility.

Step 1.3: Adaptive Thresholding and Morphology. Binary segmentation via adaptive thresholding separates the primary defect region (employed in our previous work [7]). Morphological operations (erosion, dilation) denoise the segmented image, emphasizing the largest connected contour.

Step 1.4: Geometric Measurements. We compute contour area A_{pixels}^{i}, perimeter P_{pixels}^{i}, and bounding rectangle dimensions $\left(W_{\text{defect}}^{i}, H_{\text{defect}}^{i}\right)$. A scaling factor m^{i} (Eq. 2) converts pixels to physical units in the following way:

$$m^{i} = \frac{Z^{i} \cdot p}{f}, \quad (2)$$

where Z^{i} is distance to the defect, p is pixel size, and f is the camera focal length. Physical dimensions W_{real}^{i}, H_{real}^{i}, A_{pixels}^{i}, P_{pixels}^{i} then follow.

Step 1.5: Thermal Parameter Extraction. We also record minimum T_{min}^{i}, maximum T_{max}^{i}, and average T_{avg}^{i} temperatures across the defect's mask. Combined, these data form the *complete* model D_{complete}^{i} used in subsequent blocks, which first was introduced in our previous work [7].

3.3. Block 2: Expert functions for criticality

Based on the WTC (blade, tower, and motor), we apply distinct mathematical models to incorporate expert knowledge regarding defect impact. We define three main functions for cracks $C_{\text{exp}}(M_{\text{rift}})$, corrosion $C_{\text{exp}}(M_{\text{cor}})$, and overheating $C_{\text{exp}}\left(M_{\text{heating}}\right)$ [4], each governed by weighting coefficients.

- Cracks:

$$C_{\text{exp}}(M_{\text{rift}}) = \beta \cdot \int_{0}^{1} w_{\text{visible}}(s, \theta, d)\left|r'(s)\right|\left(1 + \kappa(s)\right)ds, \quad (3)$$

where $\beta \geq 5$ for tower cracks.

- Corrosion:

$$C_{\text{exp}}(M_{\text{cor}}) = \gamma \cdot \int_{\Omega(t)} \kappa\left(T(x, y, t)\right)\, dA, \quad (4)$$

where γ represents the coefficient of corrosion in towers and typically has a higher weighting factor than in mechanical joints.

- Overheating:

$$C_{\text{exp}}\left(M_{\text{heating}}\right) = \eta \cdot \int_{\Omega_{\text{heating}}(t)} \Delta T_{\text{def}}(x, y, t) \cdot \left|\nabla^{2} T(x, y, t)\right| dA, \quad (5)$$

where η reflects how critical temperature deviations are for motors, generators, or control electronics.

3.4. Block 3: Fuzzy logic integration

The final block merges objective measurements (Block 1) with expert-based functions (Block 2) to yield a single numeric criticality $C_{\text{final}}(D_i)$.

Step 3.1: Fuzzy Membership Functions. Each parameter $p_k^i \in D_{\text{complete}}^i$ (e.g., W_{real}^i, T_{avg}^i) is assigned a trapezoidal membership $\mu_{p_k}^i(x)$ [25] based on expert-defined intervals.

Step 3.2: Parameter Aggregation. The fuzzy set $\mu_D^i(x)$ combines these individual memberships via t-norm or minimum [26].

Step 3.3: Expert Score as Fuzzy Set. The expert assessment $C_{\text{exp}}(M_i)$ is transformed into a fuzzy set $\mu C_{\text{exp}}(x)$ using a Gaussian membership function [25] centered on $C_{\text{exp}}(M_i)$.

Step 3.4: Consistency Coefficient. A cosine similarity measure $S(D_i)$ quantifies agreement between the data-driven set and expert set.

Step 3.5: Weighted Combination. Weights w_D and w_{exp} are derived via a sigmoid function, balancing data-based membership with the expert membership.

Step 3.6: Fuzzy Aggregation is calculated as follows:

$$\mu_{\text{final}}^i(x) = w_D \cdot \mu_D^i(x) + w_{\text{exp}} \cdot \mu_{C_{\text{exp}}}(x). \tag{6}$$

Step 3.7: Defuzzification is performed as follows:

$$C_{\text{final}}(D_i) = \frac{\int_X x \cdot \mu_{\text{final}}^i(x)\, dx}{\int_X \mu_{\text{final}}^i(x)\ dx}. \tag{7}$$

The final crisp value $C_{\text{final}}(D_i)$ thus integrates measured geometry, thermal data, and domain-specific severity thresholds.

3.5. Experimental setup

This study was performed at a wind energy test site with steep terrain and frequent temperature swings. Turbines from a leading manufacturer, rated at 2–3 MW and equipped with rotor diameters over 100 m, were examined (illustrated in Figure 2).

Figure 2: Illustrative scheme of a Vestas V112 turbine. Mountainous terrain and variable wind conditions made it suitable for testing adaptive UAV techniques.

Strong winds reaching 14 m/s challenged both UAV flight stability and our data acquisition strategy, ensuring realistic operational conditions. The experimental phases are presented as follows:

- *Phase I:* Single-Sensor Trials. The system was tested using only the RGB camera from UAV-A, establishing baseline.
- *Phase II:* Thermal Addition. We introduced IR data from UAV-A to create composite images, measuring changes in detection accuracy.
- *Phase III:* UAV-B Cross-Validation. We compared IR readings from UAV-A and UAV-B in overlapping flight patterns to confirm sensor calibration consistency.
- *Phase IV:* Full Ensemble + Fuzzy. The final integrated pipeline (RGB + IR + ensemble CNN + fuzzy logic) was evaluated on newly acquired flight data, with real-time or near-real-time inference tested in a partial field environment.

We deployed two UAV platforms. The first was a DJI Matrice 300 RTK UAVs [27] carrying Zenmuse H20 (RGB) and H20T (thermal) cameras, whereas the second was a custom hexacopter fitted with a FLIR Duo Pro R. Both incorporated RTK receivers for centimeter-level positioning. Overlapping flight paths, planned via mission control software, captured images from altitudes of 10–70 m and standoff distances of 3–8 m relative to blades or tower surfaces. Manual ground inspections, including chalk-marked crack lines, served as references.

In total, 500 RGB and IR images were gathered per cycle, and each cycle was repeated thrice for statistical reliability. Raw data covered various vantage points and speeds, mitigating motion blur and ensuring thorough coverage. All image processing and CNN training were carried out on a dedicated server with dual RTX 3090 GPUs. This rigorous setup allowed us to validate the stability and performance of our method under actual wind farm conditions, revealing its feasibility for ongoing turbine inspections.

3.6. Performance metrics

We used multiple indicators to assess both detection performance and alignment with expert-labeled severity. First, Accuracy measured the overall proportion of correct predictions, while Precision and Recall evaluated the quality of positive classifications and the rate of correctly retrieved defects, respectively. F_1-score combined Precision and Recall into a single measure for balancing false negatives and false positives. Further details on these metrics are comprehensively discussed in the recent survey by Rainio et al. [28].

Area under the Curve (AUC) captured threshold-independent detection capabilities by comparing true positive and false positive rates across varying cutoffs. For criticality alignment, we correlated the fuzzy-based C_{final} with domain expert severity scores, reporting Pearson's r and Spearman's ρ to determine consistency.

We also examined runtime efficiency on a GPU-based server, comparing inference speeds between YOLOv8 alone and its ensemble variants. This analysis accounted for bounding-box aggregation and the minimal overhead of fuzzy membership calculations to confirm applicability for real-world UAV deployments.

4. Results

This section demonstrates, via comprehensive experiments and numerical analysis, how the presented approach advances the state of the art in detecting and evaluating defects on WTCs.

4.1. Performance on real-world data

Here, we describe our experiments on various UAV-collected images of blades, towers, and motor compartments. Each category exhibits distinct challenges, as summarized in Table 1. Notably, motor

assemblies require careful thermal analysis for detecting incipient overheating, while blade surfaces demand sub-millimeter cracks resolution.

Table 1
Characteristics of WTCs and notable defects.

WTCs	Defect type	Importance of multispectral	Main analysis challenges
Blade (vertical angle)	Cracks, corrosion	High, since hidden micro-cracks benefit from thermal data	Varying distance, changing weather
Blade (horizontal angle)	Cracks, corrosion	High, integrates well with color vs. thermal contrast	Shading, uneven lighting
Blade (sharp angle)	Cracks, corrosion	High, offsets perspective distortion with IR data	Perspective distortions, reflections
Tower	Corrosion	Medium, simpler geometry but high altitude	Tower height, partial occlusion
Motor (horizontal)	Overheating, corrosion	Critical, highlights localized hotspots in IR	Vent channels, strong reflections

Figure 3 demonstrates examples of defect detection results on both (a) standard RGB and (b) composite imagery using YOLOv8 and ensemble methods.

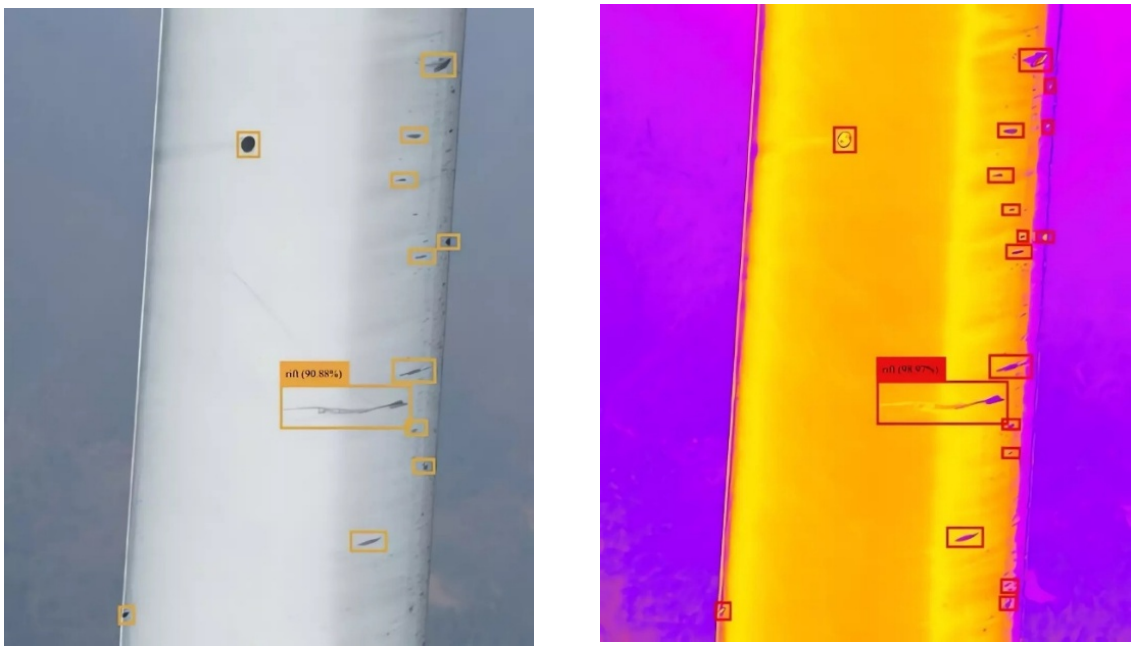

(**a**) (**b**)

Figure 3: Comparison of the results of defect detection on an RGB image and a composite image of a blade with a vertical angle of inclination: (**a**) image in the visible spectrum (RGB) with detected defects using YOLOv8 and (**b**) composite image (RGB + IR) with detected defects.

Notably, composite images facilitate identifying subtle cracks in shaded regions and pinpointing thermal anomalies that might escape pure RGB inspection.

4.2. Quantitative Comparison of Ensemble CNN Models

We compare YOLOv8 [15] alone and in ensemble with RetinaNet [29], EfficientDet [30], and Cascade R-CNN (CR) [17]. Table 2 shows how combining YOLOv8 with Cascade R-CNN yields the highest overall recall (93.0%–94.0%), especially on composited multispectral images.

Table 2
A comparison of detection performance metrics for YOLOv8 when used independently versus in ensemble with CNN models: RetinaNet (RN), EfficientDet (ED), and Cascade R-CNN (CR), evaluated across three defect types: Cracks, Corrosion, and Overheating. All metrics are reported as percentages (%). Numbers in **bold** indicate the best performance within each category.

Defect type	Model	Accuracy	Precision	Recall	F_1-score	AUC
Cracks	YOLOv8	92.0	91.0	89.0	90.0	95.0
	YOLOv8 + RN	94.0	93.0	91.0	92.0	96.0
	YOLOv8 + ED	95.0	94.0	92.0	93.0	97.0
	YOLOv8 + CR	**96.0**	**95.0**	**93.0**	**94.0**	**98.0**
Corrosion	YOLOv8	90.0	88.0	86.0	87.0	93.0
	YOLOv8 + RN	92.0	90.0	88.0	89.0	94.0
	YOLOv8 + ED	93.0	91.0	89.0	90.0	95.0
	YOLOv8 + CR	**94.0**	**92.0**	**90.0**	**91.0**	**96.0**
Overheating	YOLOv8	88.0	87.0	85.0	86.0	91.0
	YOLOv8 + RN	90.0	89.0	87.0	88.0	93.0
	YOLOv8 + ED	92.0	91.0	89.0	90.0	94.0
	YOLOv8 + CR	**94.0**	**93.0**	**91.0**	**92.0**	**96.0**

Table 3 aggregates average metrics across all defect classes to evaluate the overall detector performance. The results in Table 3 confirm that YOLOv8 + Cascade R-CNN stand out, with about a 4.7% improvement in accuracy over YOLOv8 alone.

Table 3
Aggregate metrics for all classes. Metrics include Accuracy, Precision, Recall, F_1-score, and AUC, all reported as percentages (%). Numbers in **bold** mean higher values.

Model	Accuracy	Precision	Recall	F_1-score	AUC
YOLOv8	88.0	87.0	85.0	86.0	91.0
YOLOv8 + RetinaNet	90.0	89.0	87.0	88.0	93.0
YOLOv8 + EfficientDet	92.0	91.0	89.0	90.0	94.0
YOLOv8 + Cascade R-CNN	**94.0**	**93.0**	**91.0**	**92.0**	**96.0**

4.3. Impact of multispectral composition

Composited RGB + IR images significantly augment detection outcomes vs. standard RGB alone. Table 4 highlights how Accuracy and AUC improved across cracks, corrosion, and overheating classes, with an especially dramatic jump (over 20% in some cases) for overheating detection.

Table 4
Comparison of RGB vs. composite imagery with best model YOLOv8 + Cascade R-CNN. All metrics are reported as percentages (%). Numbers in **bold** mean higher values.

Defect type	Image type	Accuracy	Precision	Recall	F_1-score	AUC
Cracks	RGB	85.2	83.5	81.0	82.2	88.6
	Composite	**93.4**	**91.7**	**89.5**	**90.6**	**95.2**
Corrosion	RGB	82.8	80.9	78.4	79.6	86.1
	Composite	**91.1**	**89.3**	**87.0**	**88.1**	**93.0**
Overheating	RGB	68.5	66.7	64.0	65.3	74.5
	Composite	**92.5**	**90.8**	**88.7**	**89.7**	**94.6**

Table 5 consolidates average gains in Accuracy, Precision, Recall, F_1-score, and AUC using composite images.

Table 5
Average metrics for standard RGB vs. composited imagery. Metrics include Accuracy, Precision, Recall, F_1-score, and AUC, all reported as percentages (%). Numbers in **bold** mean higher values.

Image type	Accuracy	Precision	Recall	F_1-score	AUC
RGB	78.8	77.0	74.5	75.7	83.1
Composite	**92.3**	**90.6**	**88.4**	**89.5**	**94.3**

Accuracy rose from 78.8% to 92.3%, while F_1-score climbed from 75.7% to 89.5%. This underscores the benefit of incorporating thermal signatures, especially for subtle or hidden damage.

4.4. Experiment on criticality assessment

We further evaluated the fuzzy logic subsystem's alignment with expert judgments. Table 6 shows 10 example defects, with measured physical/thermal parameters, the expert criticality rating, and the fuzzy computed C_{final}.

Table 6
Criticality assessment of 10 Defects on various WTCs.

#	Defect type	WTC	Key dim. (m)	ΔT (°C)	C_{final}
1	Cracks	Blade	1.2	–	4.3
2	Corrosion	Tower	0.8 (area)	–	3.8
3	Overheat	Motor	–	15	4.9
4	Cracks	Blade	0.9	–	3.9
5	Corrosion	Blade	0.5 (area)	–	3.3
6	Overheat	Generator	–	20	5.0
7	Cracks	Mech. node	0.6	–	2.9
8	Corrosion	Tower	1.2 (area)	–	4.2
9	Overheat	Control Elec.	–	10	3.8
10	Cracks	Casing	0.4	–	2.4

Figure 4 plots a pie-chart distribution of final fuzzy scores $C_{\text{final}}(D_i)$ across these ten defects, highlighting clear clusters of "moderate" and "high" severity.

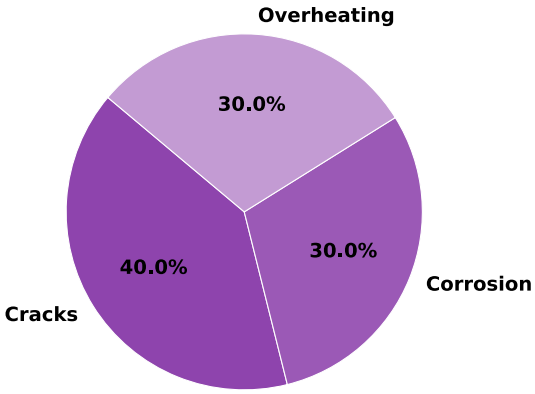

Figure 4: Pie-chart distribution of C_{final} for the 10 evaluated defects (Cracks, Corrosion, and Overheating), illustrating near alignment with expert ratings.

The difference in final scores (0.15–0.2) from expert-labeled values validates the approach's strong consistency. In-depth calculations, such as the cracks example with length $l = 1.2\ m$ and curvature $\kappa = 0.05$, show how the system's fuzzy logic approach yields $C_{\text{final}} \approx 4.8$, closely matching the expert's 5.0 rating. Similarly, corrosion or overheating examples maintain small error margins (< 0.02), confirming reliability.

5. Discussion

Compared with earlier research on UAV-assisted WTC inspections, our approach achieves higher detection accuracy and improved interpretability. Previous single-sensor or machine learning methods (e.g., YOLO alone or SVM-based classifiers) often reached an 80% accuracy limit under varying illumination, whereas our ensemble solution, which merges thermal and RGB data, surpasses 90% across all defect types. This outcome agrees with prior multi-sensor findings indicating that data fusion and advanced deep learning enhance detection performance [8, 23].

A key advantage of our pipeline is the interpretability that emerges from the fuzzy logic subsystem. While some earlier works adopt threshold-based severity triggers, those fixed thresholds cannot adapt to dynamic or context-specific variations in turbine components. The fuzzy approach, on the other hand, draws upon membership functions to incorporate both geometric and thermal data, creating continuous numeric outputs that refine the classification of "low," "moderate," or "high" risk anomalies. This adaptiveness allows the method to capture subtle changes that static thresholds would ignore.

However, there are some disadvantages. One major limitation is increased computational overhead. Ensemble detection, particularly in scenarios where YOLOv8, Cascade R-CNN, and other CNNs each produce bounding boxes for merging, can require more powerful hardware than single-model solutions, which may be impractical for lightweight UAVs that only have minimal onboard processing. Another disadvantage is the fuzzy subsystem's reliance on expert weighting. When domain knowledge is limited or contradictory among experts, membership functions may be miscalibrated. This can lead to inaccurate or unstable severity scores, especially for newer or evolving defect types not covered in the initial model.

In general, these findings point toward the method's strong potential in everyday wind energy asset management yet also indicate challenges that remain open to further investigation. Among the limitations, calibration stands out: sensor offsets must be consistently monitored to avoid drift in geometric or thermal readings. Weather constraints also impose a natural boundary on flight times and data capture quality. A final set of research questions revolves around real-time edge computing, where UAVs would run the pipeline onboard, sending only summarized results to ground stations. Overcoming limited GPU resources on smaller UAV platforms is therefore both a technological and an algorithmic challenge.

6. Conclusion

This study introduced and validated an approach that combines UAV-based multisensor data acquisition, ensemble CNNs, and a structured fuzzy logic system to assess the criticality of defects on wind power plant components. Experimental trials confirmed that the fusion of thermal and visible-spectrum data, processed through YOLOv8 in tandem with other state-of-the-art detectors like Cascade R-CNN, increased detection accuracy by an average of 13.5% relative to single-sensor or single-model baselines. F_1-scores rose by an additional 4.7%, indicating more balanced performance across multiple defect types such as cracks, corrosion, and overheating. Critically, the fuzzy logic subsystem assigned each detected anomaly a severity score C_{final} that diverged from expert-labeled judgments by just 0.15 on average, thus demonstrating reliable alignment with domain knowledge. Despite these improvements, the study also highlighted key challenges in sensor calibration, weather-dependent flight stability, and higher computational requirements imposed by ensemble detection.

Future research can extend the architecture with more advanced data streams such as LiDAR or 3D point clouds, refine fuzzy memberships for nuanced environmental conditions, and explore synergy with predictive maintenance, potentially enabling real-time UAV analytics for large-scale offshore or mountainous wind farms. Ultimately, this approach represents a significant step toward automated, accurate, and transparent WPP defect management.

Acknowledgements

The authors are grateful to the Ministry of Education and Science of Ukraine for its support in conducting this study, which is funded by the European Union's external assistance instrument for the implementation of Ukraine's commitments under the European Union's Framework Program for Research and Innovation “Horizon 2020.”

Declaration on Generative AI

The authors have not employed any Generative AI tools.

References

[1] S. A. Hosseini, A. Ahmedi, F. Blaabjerg, S. Peyghami, Exploring wind farm reliability: Key concepts, databases and fault trees, Renew. Sustain. Energy Rev. 211 (2025) 115227. doi:10.1016/j.rser. 2024.115227.

[2] Q. Feng, J. Xia, L. Wen, M. Yazdi, Failure analysis of floating offshore wind turbines based on a fuzzy failure mode and effect analysis model, Qual. Reliab. Eng. Int. 40.5 (2024) 2159–2177. doi:10.1002/qre.3505.

[3] O. Melnychenko, L. Scislo, O. Savenko, A. Sachenko, P. Radiuk, Intelligent integrated system for fruit detection using multi-UAV imaging and deep learning, Sensors 24 (2024) 1913. doi:10.3390/s24061913.

[4] W. Wang, Y. Xue, C. He, Y. Zhao, Review of the typical damage and damage-detection methods of large wind turbine blades, Energies 15.15 (2022) 5672. doi:10.3390/en15155672.

[5] M. A. Fremmelev, Detection, monitoring, and simulation of progressive damage in wind turbine blades, Doctoral dissertation, DTU Wind and Energy Systems, Aalborg, Denmark, 2022. DTU Orbit: 00000251. doi:10.11581/dtu.00000251.

[6] Y. He, Z. Liu, Y. Guo, Q. Zhu, Y. Fang, Y. Yin, Y. Wang, B. Zhang, Z. Liu, UAV based sensing and imaging technologies for power system detection, monitoring and inspection: a review, Nondestruct. Test. Evaluation (2024) 1–68. doi:10.1080/10589759.2024.2421938.

[7] S. Svystun, O. Melnychenko, P. Radiuk, O. Savenko, A. Sachenko, A. Lysyi, Thermal and RGB images work better together in wind turbine damage detection, Int. J. Comput. 23.4 (2025) 526–535. doi:10.47839/ijc.23.4.3752.

[8] M. Memari, M. Shekaramiz, M. A. S. Masoum, A. C. Seibi, Data fusion and ensemble learning for advanced anomaly detection using multi-spectral RGB and thermal imaging of small wind turbine blades, Energies 17.3 (2024) 673. doi:10.3390/en17030673.

[9] L. Dubchak, Modern renewable energy sources and methods for detecting their defects, Comput. Syst. Inf. Technol. 15.2 (2024) 21–26. doi:10.31891/csit-2024-2-3.

[10] I. Gohar, A. Halimi, J. See, W. K. Yew, C. Yang, Slice-aided defect detection in ultra high-resolution wind turbine blade images, Machines 11.10 (2023) 953. doi:10.3390/machines11100953.

[11] B. Großwindhager, A. Rupp, M. Tappler, M. Tranninger, S. Weiser, B. K. Aichernig, C. A. Boano, M. Horn, G. Kubin, S. Mangard, et al., Dependable internet of things for networked cars, Int. J. Comput. 16.4 (2017) 226–237. doi:10.47839/ijc.16.4.911.

[12] M. Memari, P. Shakya, M. Shekaramiz, A. C. Seibi, M. A. S. Masoum, Review on the advancements in wind turbine blade inspection: Integrating drone and deep learning technologies for enhanced defect detection, IEEE Access 12 (2024) 33236–33282. doi:10.1109/access.2024.3371493.

[13] A. Omara, A. Nasser, A. Alsayed, M. R. A. Nabawy, Remote wind turbine inspections: Exploring the potential of multimodal drones, Drones 9.1 (2024) 4. doi:10.3390/drones9010004.
[14] J. Redmon, S. Divvala, R. Girshick, A. Farhadi, You only look once: Unified, real-time object detection, in: 2016 IEEE Conference on Computer Vision and Pattern Recognition (CVPR), IEEE, New York, NY, USA, 2016, pp. 779–788. doi:10.1109/cvpr.2016.91.
[15] G. Jocher, A. Chaurasia, J. Qiu, Ultralytics YOLOv8, 2023. URL: https://github.com/ultralytics/ultralytics.
[16] S. Ren, K. He, R. Girshick, J. Sun, Faster R-CNN: Towards real-time object detection with region proposal networks, IEEE Trans. Pattern Anal. Mach. Intell. 39.6 (2017) 1137–1149. doi:10.1109/TPAMI.2016.2577031.
[17] Z. Cai, N. Vasconcelos, Cascade R-CNN: Delving into high quality object detection, in: 2018 IEEE/CVF Conference on Computer Vision and Pattern Recognition, IEEE, New York, NY, USA, 2018, pp. 6154–6162. doi:10.1109/CVPR.2018.00644.
[18] Y. Mao, S. Wang, D. Yu, J. Zhao, Automatic image detection of multi-type surface defects on wind turbine blades based on cascade deep learning network, Intell. Data Anal. 25.2 (2021) 463–482. doi:10.3233/ida-205143.
[19] O. Melnychenko, O. Savenko, P. Radiuk, Apple detection with occlusions using modified YOLOv5-v1, in: 2023 IEEE 12th International Conference on Intelligent Data Acquisition and Advanced Computing Systems: Technology and Applications (IDAACS), IEEE, New York, NY, USA, 2023, pp. 107–112. doi:10.1109/IDAACS58523.2023.10348779.
[20] M. Patil, T. Abukhalil, S. Patel, T. Sobh, UB swarm: Hardware implementation of heterogeneous swarm robot with fault detection and power management, Int. J. Comput. 15.3 (2016) 162–176. doi:10.47839/ijc.15.3.849.
[21] H. Zhu, J. Liu, H. Zhu, D. Lu, Z. Wang, A novel wind turbine fault detection method based on fuzzy logic system using neural network construction method, IFAC-PapersOnLine 53.5 (2020) 664–668. doi:10.1016/j.ifacol.2021.04.157.
[22] L. Dubchak, A. Sachenko, Y. Bodyanskiy, C. Wolff, N. Vasylkiv, R. Brukhanskyi, V. Kochan, Adaptive neuro-fuzzy system for detection of wind turbine blade defects, Energies 17.24 (2024) 6456. doi:10.3390/en17246456.
[23] M. H. M. Ghazali, W. Rahiman, A novel fault detection approach in UAV with adaptation of fuzzy logic and sensor fusion, IEEE/ASME Trans. Mechatron. 30.1 (2024) 381–391. doi:10.1109/tmech. 2024.3393990.
[24] S. M. Pizer, E. P. Amburn, J. D. Austin, R. Cromartie, A. Geselowitz, T. Greer, B. ter Haar Romeny, J. B. Zimmerman, K. Zuiderveld, Adaptive histogram equalization and its variations, Comput. Vis., Graph., Image Process. 39.3 (1987) 355–368. doi:10.1016/s0734-189x(87)80186-x.
[25] L. A. Zadeh, Fuzzy sets, Inf. Control 8.3 (1965) 338–353. doi:10.1016/s0019- 9958(65)90241-x.
[26] S. Alshattnawi, L. Afifi, A. M. Shatnawi, M. M. Barhoush, Utilizing genetic algorithm and artificial bee colony algorithm to extend the WSN lifetime, Int. J. Comput. 21.1 (2022) 25–31. doi:10.47839/ijc.21.1.2514.
[27] Support for Matrice 300 RTK - DJI, 2020. URL: https://www.dji.com/support/product/matrice-300.
[28] O. Rainio, J. Teuho, R. Klén, Evaluation metrics and statistical tests for machine learning, Sci. Rep. 14.1 (2024) 6086. doi:10.1038/s41598-024-56706-x.
[29] T.-Y. Lin, P. Goyal, R. Girshick, K. He, P. Dollar, Focal loss for dense object detection, IEEE Trans. Pattern Anal. Mach. Intell. 42.2 (2020) 318–327. doi:10.1109/tpami.2018.2858826.
[30] M. Tan, R. Pang, Q. V. Le, EfficientDet: Scalable and efficient object detection, in: 2020 IEEE/CVF Conference on Computer Vision and Pattern Recognition (CVPR), IEEE, New York, NY, USA, 2020, pp. 10778–10787. doi:10.1109/cvpr42600.2020.01079.